ACS APPLIED MATERIALS & INTERFACES

www.acsami.org

Research Article

Analyte-Induced Desert Rose-like Ag Nanostructures for Surface-Enhanced Raman Scattering-Based Biomolecule Detection and Imaging

Hee-Kyung Na,[⊥] Jisun Ki,[⊥] Minh-Uyen Le, Kyoung-Shim Kim, Chul-Ho Lee, Tae Geol Lee,* and Jung-Sub Wi*

Cite This: *ACS Appl. Mater. Interfaces* 2021, 13, 58393−58400

Read Online

ACCESS | Metrics & More | Article Recommendations | Supporting Information

ABSTRACT: Biomolecule detection based on surface-enhanced Raman scattering (SERS) for application to biosensors and bio-imaging requires the fabrication of SERS nanoprobes that can generate strong Raman signals as well as surface modifications for analyte-specific recognition and binding. Such requirements lead to disadvantages in terms of reproducibility and practicality, and thus, it has been difficult to apply biomolecule detection utilizing the advantages of the SERS phenomenon to actual clinically relevant analysis. To achieve reproducible and practical SERS signal generation in a biomolecule-specific manner without requiring the synthesis of nanostructures and their related surface modification to introduce molecules for specific recognition, we developed a new type of SERS probe formed by enzyme reactions in the presence of Raman reporters. By forming unique plasmonic structures, our method achieves the detection of biomolecules on chips with uniform and stable signals over long periods. To test the proposed approach, we applied it to a SERS-based immunohistochemistry assay and found successful multiplexed protein detection in brain tissue from transgenic mice.

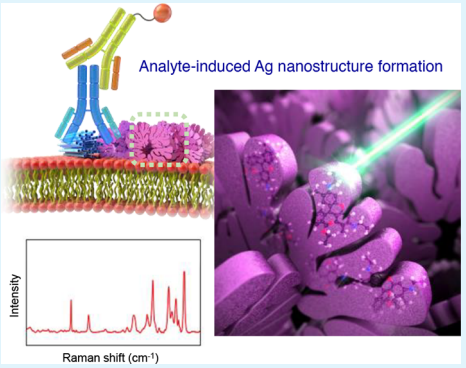

KEYWORDS: *analyte-specific SERS nanoprobe formation, multiplexed SERS imaging, SERS immunohistochemistry, desert rose-like Ag nanostructures, SERS biosensor*

INTRODUCTION

The surface-enhanced Raman scattering (SERS) phenomenon is attracting increased interest in bioanalytical applications due to its advantages in sensitivity, stable signals resistant to photobleaching for long-term monitoring, and multiplexing capability with single wavelength excitation.[1−3] Since the electromagnetic enhancement mechanism contributes greatly to SERS enhancement, various noble metal and metalloid nanostructures have been developed and applied to biomolecular detection.[4,5] A wide range of nanostructure-based SERS-active substrates and probes have been developed to generate strong Raman signals for the detection of biomolecules in both direct and indirect manners.[6−23] Despite the excellent sensitivity of the direct approach (referred to as label-free detection), issues in applying related biosensors include reproducibility, on account of the difficulty to position the Raman reporters or biomolecules inside a highly localized field, and quantification, due to the presence of electric field gradients in hot spots.[7−10]

In the case of the indirect method (which can be referred to as labeled detection based on SERS tags), various types of biomolecules can be detected with high sensitivity, specificity, and multiplexity. However, this approach requires the formation of highly complicated nanostructures.[11−16] The fabrication of such SERS nanoprobes necessitates one or more of the following: the synthesis of plasmonic nanoparticles containing a precisely controlled nanogap, the conjugation of Raman reporter molecules and antibodies, and often in the case of silver nanostructures, a protective shell for stabilization.[10,17−19] Furthermore, the sizes of these types of nanoprobes, on the scale of tens to a hundred nanometers, are often larger than the detection antibodies, which interferes with the efficient molecular recognition of the antigens on the sensors or tissues. Considering the above issues, to date, the realization of more practical applications of biosensing that utilize SERS is limited, as it has remained a challenge to create a plasmonically enhanced electromagnetic field on the nanostructures that is uniform, reproducible, and target-specific.[16,20−23]

Received: September 29, 2021
Accepted: November 19, 2021
Published: November 30, 2021

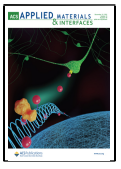

https://doi.org/10.1021/acsami.1c18815
ACS Appl. Mater. Interfaces 2021, 13, 58393−58400

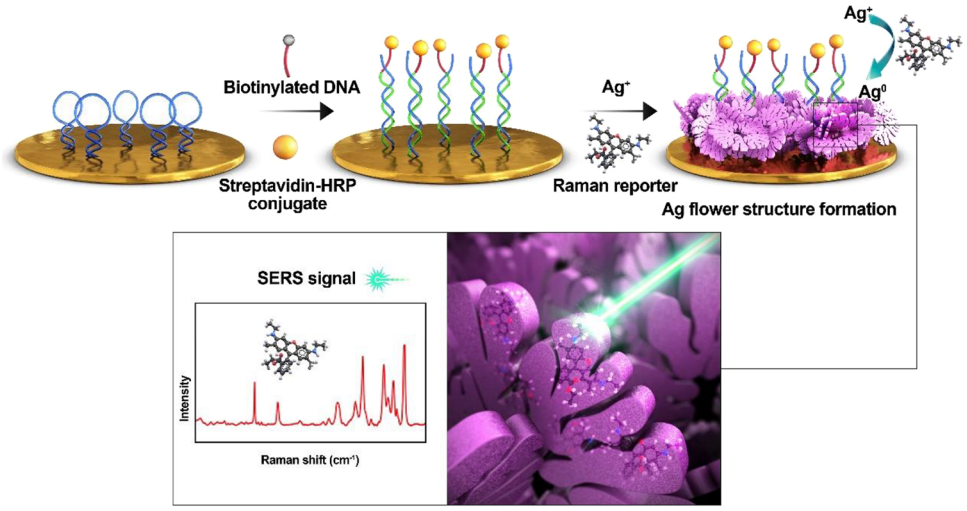

Figure 1. Schematic representation of analyte-induced Ag structure formation. The presence of target biomolecules specifically recruits HRP-streptavidin followed by an enzymatic reaction that converts Ag^+ ions to Ag structures containing Raman reporters.

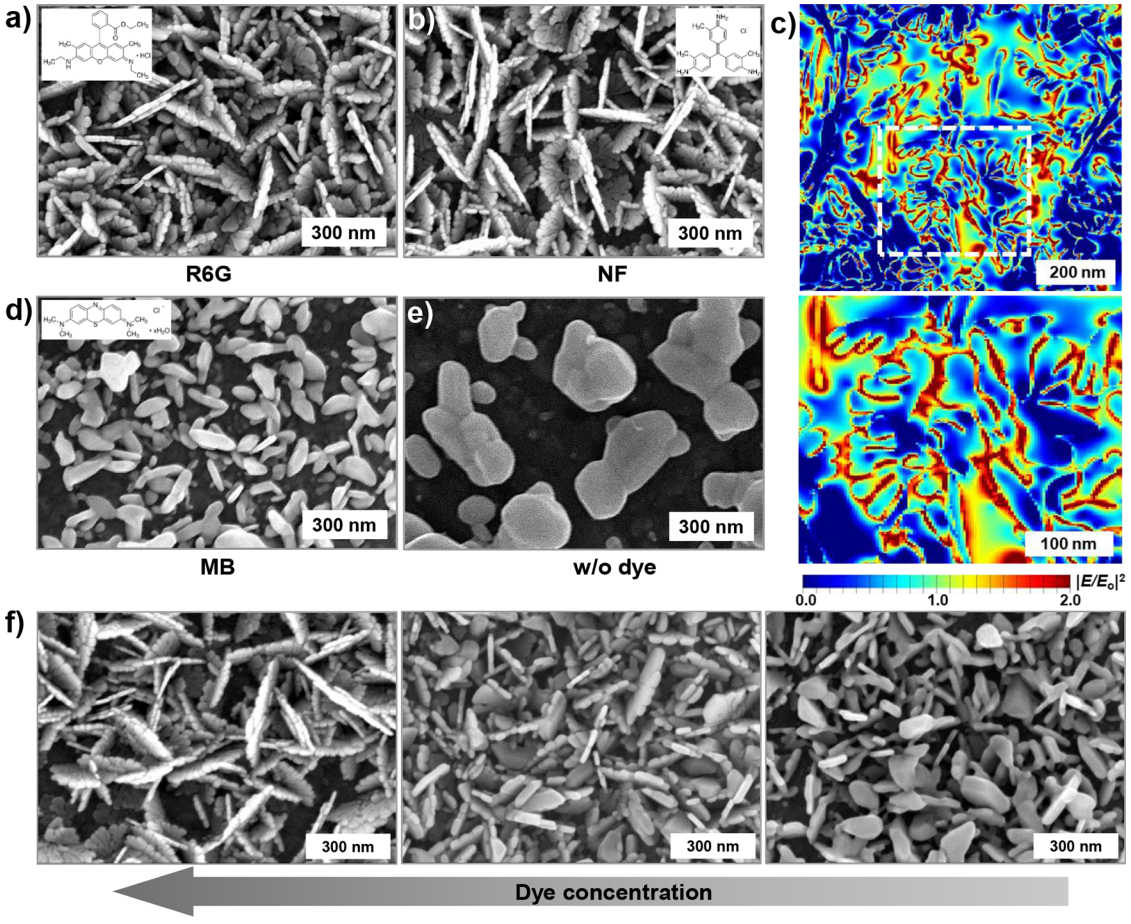

Figure 2. (a, b) SEM images of Ag nanostructures formed by HRP in the presence of (a) rhodamine 6G (R6G) and (b) new fuchsin (NF). (c) Simulated local field distributions around the desert rose-like Ag nanostructures in (b) calculated from FDTD at 532 nm excitation laser wavelength. The lower panel is a magnification of the white dashed box in the upper panel. (d, e) SEM images of Ag nanostructures formed by HRP (d) in the presence of methylene blue and (e) in the absence of a Raman reporter. (f) Structural changes by diluting the NF concentration from 0.2 mM (left) by 10 (middle) and 100 (right) times.

To meet these needs with an advanced yet practical technology, we developed a SERS nanoprobe capable of versatile application that can expand various bioassays conventionally performed with colorimetric or fluorescence analysis to SERS-based assays by forming plasmonic nanostructures with enzymes widely used in molecular biology. To provide a straightforward route for placing target and Raman reporter molecules in hot spots, here, we first present

https://doi.org/10.1021/acsami.1c18815
ACS Appl. Mater. Interfaces 2021, 13, 58393−58400

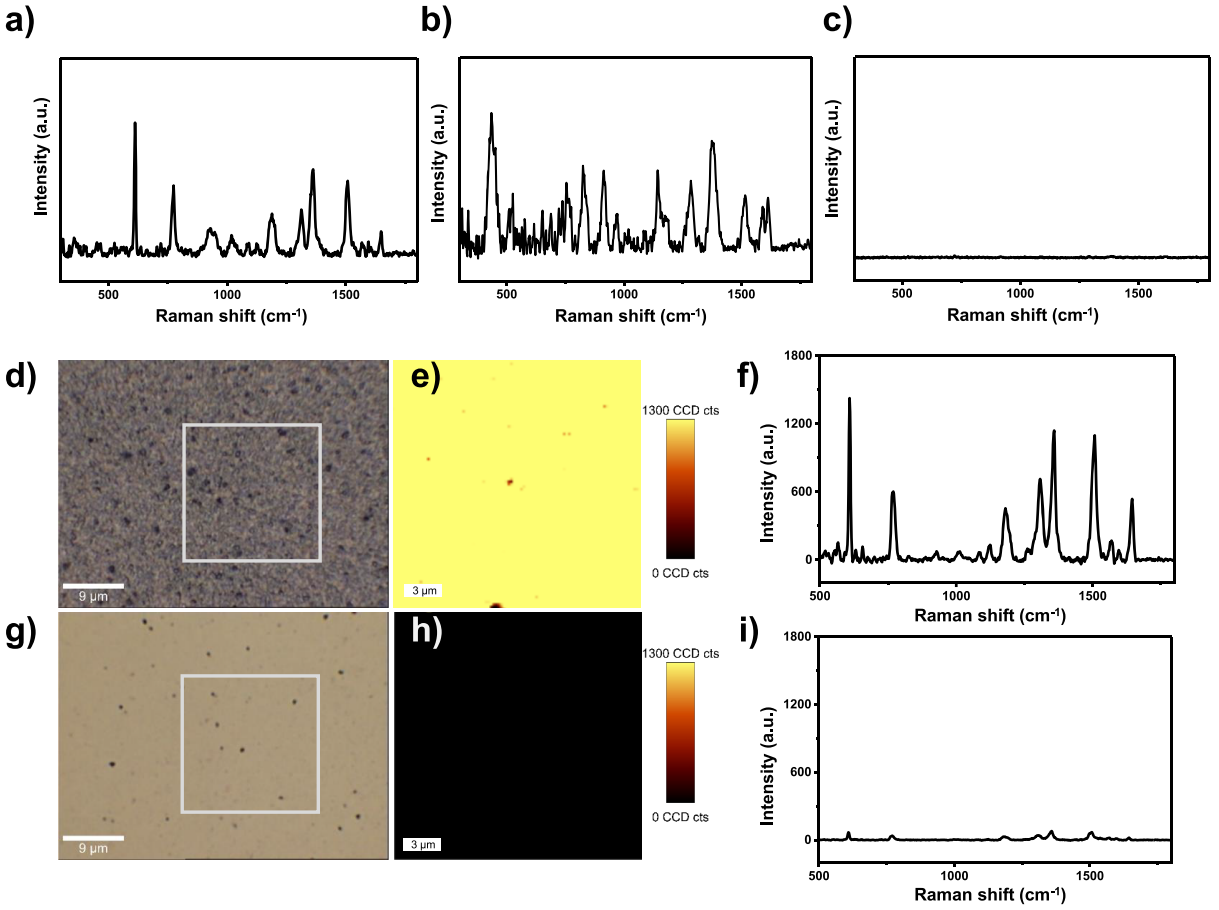

Figure 3. (a–c) Raman spectra of the Ag nanostructures synthesized in the presence of (a) R6G and (b) NF and (c) in the absence of Raman reporter. (d–i) Raman measurements in the (d–f) presence and (g–i) absence of miR-let7a. From the marked areas in the images in (d) and (g), 615 cm^{-1} Raman mapping images are shown in (e) and (h), respectively, from which the corresponding average Raman spectra is extracted in (f) and (i).

our method for the formation of unique silver nanostructures in a target-specific manner in the presence of an enzyme and Raman reporters and then report an application to a SERS-based biomolecule detection platform, the results of which demonstrate both uniformity and long-term stability of the Raman signals. The developed approach also achieves the detection of multiple proteins in tissues with single wavelength excitation.

RESULTS AND DISCUSSION

To achieve target-specific SERS probe formation, we designed a sensing scheme in which the horseradish peroxidase (HRP) enzyme only binds to the sensor surface in the presence of an analyte, as shown in Figure 1. Since HRP is known to participate in Ag^+ ion reduction,[24,25] it was expected to form plasmonic structures that could be utilized as a SERS probe. Prior to application for biomolecule detection, a gold substrate immobilized with HRP was prepared in order to verify the characteristics of the Ag structure formation by HRP in the presence of Ag^+ ions, hydroquinone, and H_2O_2.[24] In addition, rhodamine 6G (R6G), a chromophore commonly used in SERS sensors due to its inherently large Raman cross section, was treated together with the enzyme to generate strong Raman signals from the Raman reporters within the plasmonic structures. Interestingly, in the presence of R6G at 0.2 mM concentration, we found that unique desert rose-like Ag nanostructures containing abundant nanogaps were formed, as shown in Figure 2a. In order to examine the effect of Raman reporters on the formed nanostructures, several types of Raman reporters were processed, where it was found that new fuchsin (NF) and basic fuchsin (BF) also formed similar structures to R6G, as shown in Figure 2b and Figure S1. On the other hand, methylene blue (MB), which is widely used as a Raman reporter, was found not to produce the desert rose-like structures, being rather similar to the case in which no Raman reporter is present, as shown in Figure 2d,e. To check the effect of Raman reporter concentration, we diluted the Raman reporters by 10 and 100 times and found irregular and unstable structures, as shown in Figure 2f, indicating that the presence of the Raman reporter is critical in forming the unique Ag nanostructures. As described elsewhere, interactions between a Ag seed surface and Raman reporter such as R6G, NF, or BF are expected to alter the growth kinetics of preferential Ag flowers (or plates) in forming interlaced clusters with numerous nanogaps,[26–29] a phenomenon that we observe here in the different structures formed by different Raman reporters in Figure 2a–e and Figure S1. As shown in Figure 2 and Figure S2, Ag structures formed by treatment with various dyes with similar core structures but containing various substituents were examined. Since intermolecular interactions between molecules used as templates also affect the morphology of nanostructures,[30] the bulkiness and charge of the substituents seem to affect the formation of the desert

https://doi.org/10.1021/acsami.1c18815
ACS Appl. Mater. Interfaces 2021, 13, 58393–58400

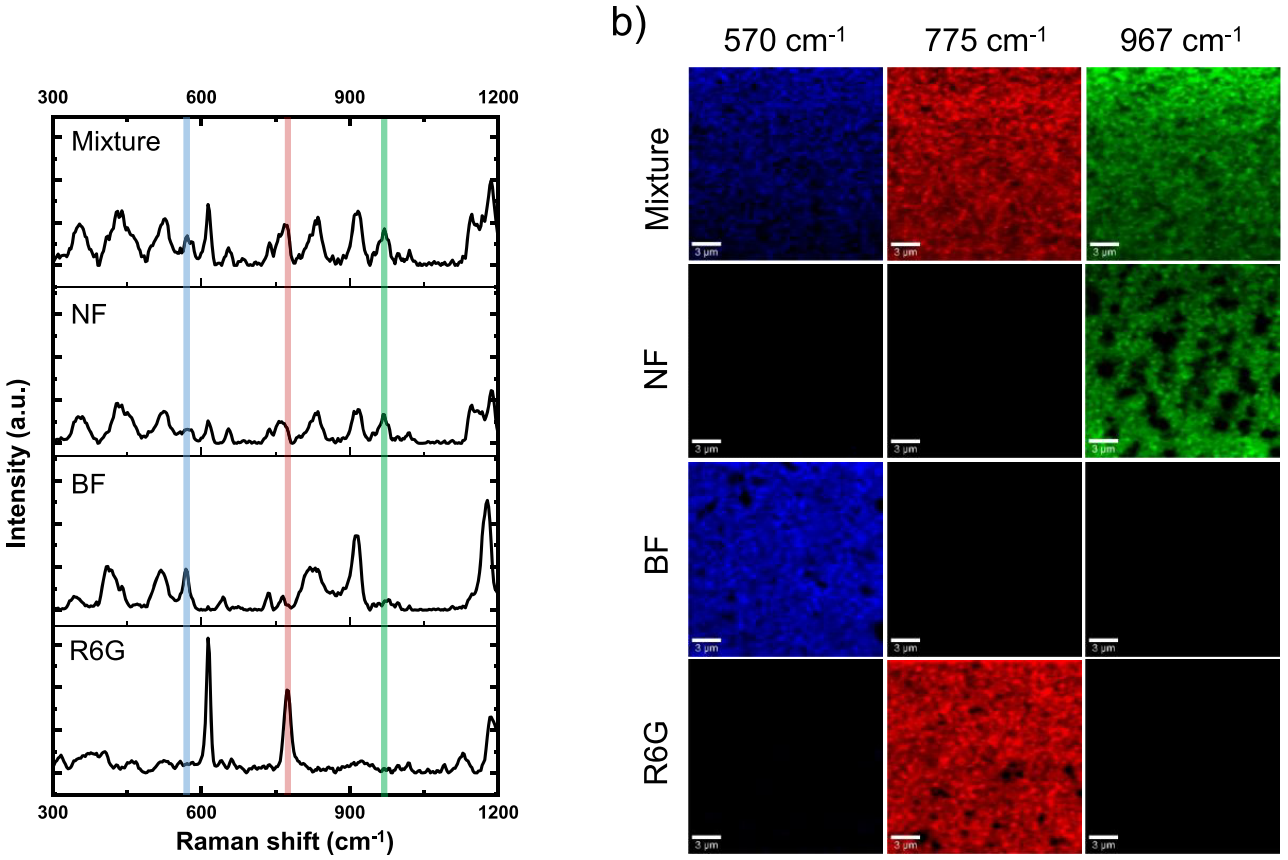

Figure 4. Multiplexed detection using NF-, basic fuchsin (BF)-, and R6G-treated Ag nanostructures. (a) Raman spectra of each Raman reporter contained in nanostructures and that of a co-treated one (top). (b) Raman images obtained by mapping at 570 cm^{-1} (blue, characteristic peak of BF), 775 cm^{-1} (red, characteristic peak of R6G), and 967 cm^{-1} (green, characteristic peak of NF).

rose-like Ag structures here. In addition, changes in the structure of the Raman reporter through reactions with the Ag ions and HRP present in the solution may also affect the formation of the Ag nanostructures. In particular, MB is a molecule known to easily undergo charge and structural changes by participating in oxidation/reduction reactions.[31] Consequently, it seems to be affected by intermolecular interaction and binding with Ag seeds, so that it does not function properly here as a template.

Formed through Ag^+ ion reduction in the presence of HRP and a Raman reporter, the plasmonic nanoflower structures with numerous nanogaps were expected to generate a considerable Raman signal. Accordingly, we investigated the potential of the nanostructures to be employed as SERS probes. The enhanced electromagnetic fields around the Ag nanostructures were simulated using three-dimensional finite-difference time-domain software (Lumerical FDTD solution). For a reliable modeling of the Ag nanostructures, the contrast-enhanced SEM image shown in Figure 2b was imported and set to have a 100 nm thickness. The modeled Ag nanostructure was exposed to a plane wave of 532 nm with the same wavelength used in the SERS experiments in our study. More detailed simulation conditions are described in the Materials and Methods section. Figure 2c shows the calculated contours of $|E/E_o|$,[2] where E_o and E are the amplitude of the incident and enhanced electric fields. Highly enhanced electric fields, represented by the red colored regions, can be seen to be distributed in the spaces between neighboring Ag nanostructures, as shown in the upper panel of Figure 2c, as well as in the internal spaces of a single nanostructure, as shown in the magnification (lower panel) of Figure 2c. As presented in both simulation images, the Ag nanoflowers provide numerous hot spots with enhanced electric fields. The simulation results also show that the average value of $|E/E_o|$,[4] which has been shown to be comparable with SERS enhancement factors,[32] is about 2×10^4. This enhancement factor is high enough for the Raman signals of the reporter molecules incorporated into the Ag nanostructures to be detected.

By the formation of the Ag structures with Raman reporter molecules, the presence of the target analyte could be easily identified via its characteristic Raman spectrum, as shown in Figure 3a–c. To see the potential for biomolecule detection, a thiol-modified DNA probe for capturing miRNA was immobilized on a gold wafer. Referring back to the sensing strategy in Figure 1, detection probe hybridization was followed by HRP binding to induce the formation of a SERS probe that produces strong Raman signals in the presence of miR-let7a at 100 nM concentration. It is worth noting that it is difficult to form analyte-specific SERS nanoprobes in the presence of a surface capture probe since it is known that the base structure of DNA is involved in the formation of unique Ag structures controlling the morphological evolution of the nanoparticle growth by different interactions between the Ag seed and each base.[33,34] We had the idea of fixation to remove the interfering molecule in the Ag staining process, and we treated with paraformaldehyde before the reagent treatment for the Ag nanostructure formation reaction. Through this, we were able to induce target-specific Raman signal generation, as

https://doi.org/10.1021/acsami.1c18815
ACS Appl. Mater. Interfaces 2021, 13, 58393−58400

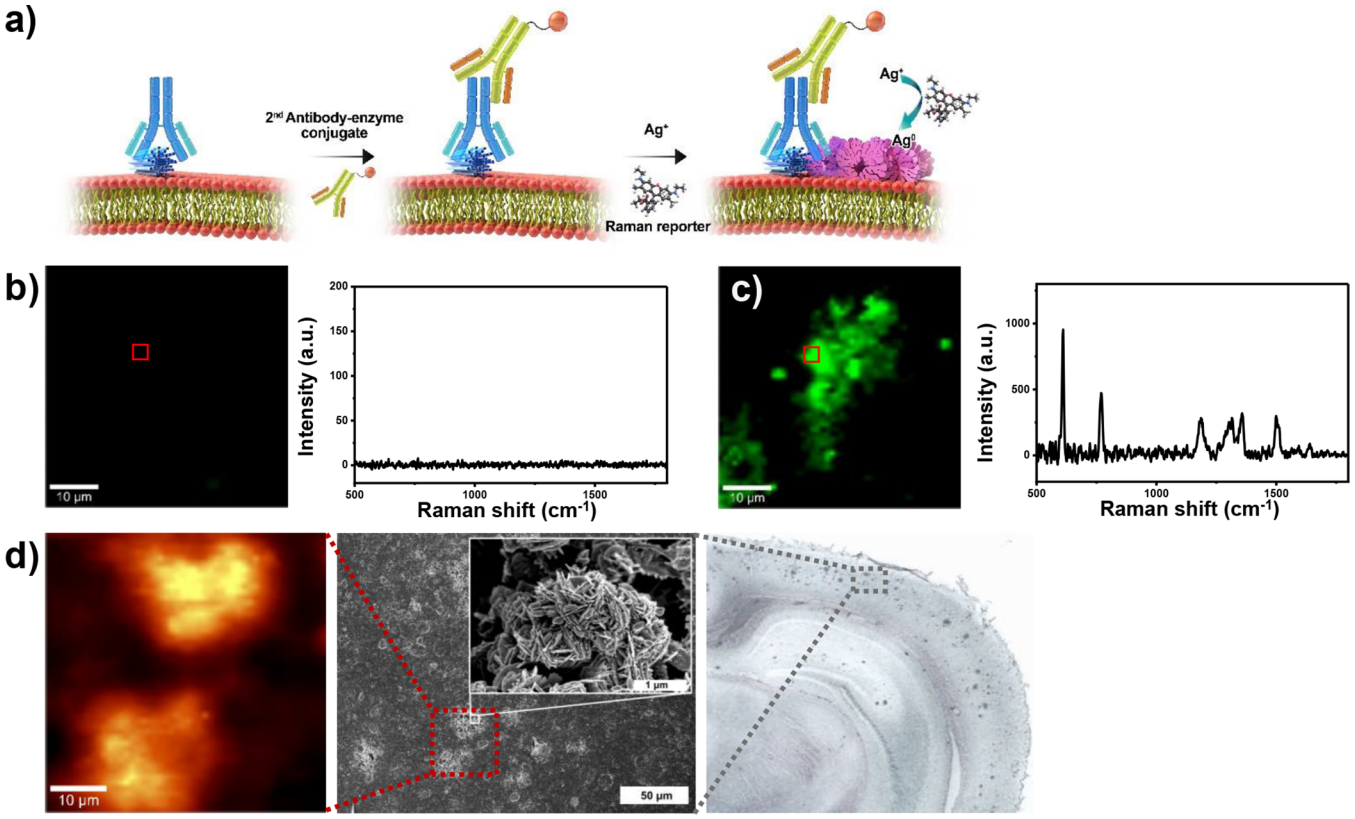

Figure 5. SERS-based immunohistochemistry assay. (a) Schematic representation of Ag nanostructure formation on tissue. (b) Raman mapping image at 775 cm^{-1} from wild-type mouse brain tissue (left) and corresponding Raman spectrum (right) extracted from the region-of-interest (ROI). (c) Raman mapping image at 775 cm^{-1} from APP/PS1 transgenic mouse brain tissue (left) and corresponding Raman spectrum (right) extracted from the ROI. (d) Raman mapping image at 775 cm^{-1} (left), SEM images (middle), and optical image (right) of APP/PS1 transgenic mouse brain tissue after staining with the anti-β-amyloid antibody and R6G.

shown in Figure 3d–i. Also, in the case of point analysis of the SERS biosensor, since a large point-to-point variation can affect the reproducibility and accuracy of measurement, we employed a Raman imaging technique in which all the pixel points with characteristic Raman peaks (615 cm^{-1}) are mapped over a 20 μm × 20 μm area with an excitation laser wavelength of 532 nm.[35] The Raman mapping results in the marked areas of Figure 3d,g are shown in Figure 3e,h, which are plotted with the same color intensity scale, and are clearly different. The average SERS signals from the mapping areas in Figure 3e,h are shown in Figure 3f,i, respectively. Comparing Figure 3f to Figure 3i confirms that a strong Raman signal was observed only when the target was present. Signal intensity changes by miR-let7a concentration were observed in the Raman mapping images at 615 cm^{-1} in Figure S3. The Raman spectra in Figure S4 show that miR-let7a was detected up to 1 fM. The two-dimensional maps of Raman intensities in Figure 3e and Figure S3 show distinct visible evidence of the uniform and reproducible spatial distribution of the Raman signal. Finally, it is worth mentioning that our SERS nanoprobe provided the same signal intensity stably over a long period of time. As shown in Figure S5, the SERS nanoprobe formed with NF provided a strong and stable signal intensity for up to 3 months. The stability of SERS signals allows for repetitive measurements that enhance reproducibility and reduce test errors.[22,36]

Next, to investigate the potential of the developed approach for multiplexed detection and imaging, the nanostructures were first formed in the presence of various Raman reporters. Raman spectra were then obtained, as shown in Figure 4a, after the immobilization of HRP on a gold wafer followed by treatment with R6G, BF, and NF and a co-treatment of the three Raman reporters with Ag ions. The Raman peaks at 570, 775, and 967 cm^{-1} corresponding to BF (blue), R6G (red), and NF (green), respectively, were used to obtain the Raman mapping images in Figure 4b over a 20 μm × 20 μm area with an excitation laser wavelength of 532 nm. Figure 4a,b shows that the Raman peaks of each probe as well as the images could be clearly distinguished in the plasmonic Ag nanoflowers produced by treatment with the three types of Raman reporters together, compared to those by treatment with individual Raman reporters.

Finally, we applied our straightforward SERS nanoprobe to an immunohistochemistry assay to check whether it is possible to detect multiple proteins in tissues, as schematically shown in Figure 5a. We tried to detect β-amyloid, known as a major neuropathological feature of Alzheimer's disease,[37] in brain tissue from wild type and APP/PS1 transgenic mice at 9 months. In Figure 5b,c, with the same color intensity scale, strong Raman signals were observed in the brain tissue from the APP/PS1 mice treated with the anti-β-amyloid antibody and R6G. The spectrum extracted from the region-of-interest (ROI) showed distinguishable Raman peaks compared to the signal obtained from the wild-type brain tissue. In the Raman mapping image in Figure 5d, β-amyloid deposition in the cortex of the transgenic mouse brain is clearly observed. In addition, the desert rose-like Ag nanostructures were found in SEM images of the tissue, as shown in Figure 5d and Figure S3.

https://doi.org/10.1021/acsami.1c18815
ACS Appl. Mater. Interfaces 2021, 13, 58393−58400

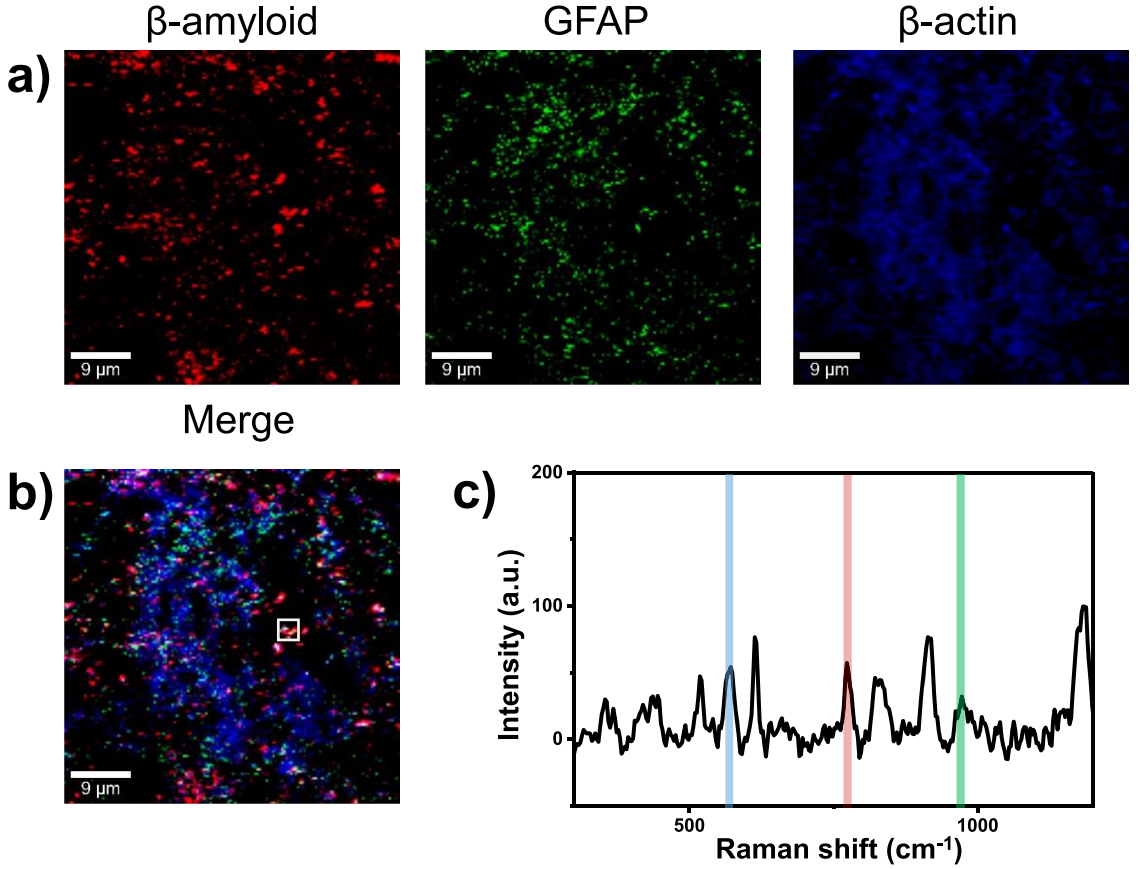

Figure 6. (a, b) Multiplexed Raman imaging of proteins in APP/PS1 transgenic mouse brain tissue. The Raman images were obtained after multiple immunostainings with antibodies against β-amyloid, GFAP (astrocyte marker), and β-actin from each characteristic Raman peak at 775 cm^{-1} (red, characteristic peak of R6G), 967 cm^{-1} (green, characteristic peak of NF), and 570 cm^{-1} (blue, characteristic peak of BF), respectively. The image in (b) is a merged image. (c) Corresponding Raman spectrum extracted from the ROI.

In order to verify that the SERS probe that we developed is capable of multiplexed assays for biomolecule detection in real tissues, immunostaining was performed using antibodies against β-amyloid, glial fibrillary acidic protein (GFAP) known to be expressed in astrocytes,[38] and β-actin, a well-known endogenous housekeeping protein, as shown in Figure 6. In the brain tissue from APP/PS1 mice, by the treatment of the secondary antibody labeled with HRP followed by treatments of Ag^+ and each Raman reporter, the SERS nanoprobes were formed successfully without requiring any pre-fabricated nanostructures. Clear Raman signals were obtained at 775 cm^{-1} (characteristic peak of R6G) corresponding to β-amyloid (red), 967 cm^{-1} (characteristic peak of NF) corresponding to GFAP (green), and 570 cm^{-1} (characteristic peak of BF) corresponding to β-actin (blue); as shown in Figure 6c, the Raman spectrum extracted from the ROI showed distinguishable characteristic peaks from the SERS probes for each protein.

In general, for multiplexed immunodetection in SERS, several processes are required including the synthesis of a uniform nanostructure, introduction of different types of Raman reporters, and antibody conjugations according to the molecules to be detected.[39,40] In contrast, without any of these processes, we were able in this work to easily implement multiplexed SERS immunodetection by treating each Raman reporter with commercially available antibody combinations.

CONCLUSIONS

We developed an approach to analyte-induced SERS nanoprobe formation that provides both uniform and long-term stable Raman signals. Our strategy does not require the synthesis or surface modification of nanostructures with Raman reporters or capture/detection probes. It was shown that biomolecules can be detected both on chip and in tissue through the formation of enzyme-specific plasmonic nanostructures. By forming a desert rose-like nanostructure using a Raman reporter and HRP, an enzyme widely used in the field of biology, a new methodology was presented here that can convert various existing bioassays including the sandwich immunoassay, hybridization-based gene sensing, immunohistochemistry, and *in situ* hybridization into SERS-based assays.

MATERIALS AND METHODS

Materials. DNA probes were purchased from Genotech (Daejeon, Republic of Korea) with the following sequences: capture probe, 5′-thiol(C6)-GGC AAC TAT ACA ACC TAC TAC CTC ATA TAG TTG CC-3′; signal probe, 5′-biotin-GGC AAC TAT A-3′. MicroRNA (miR-let7a) was purchased from Bioneer (Daejeon, Republic of Korea) with the same sequences as a previous report.[31] Phosphate-buffered saline (PBS) was purchased from WelGene (Gyeongsan, Republic of Korea). Streptavidin-HRP conjugate, bovine serum albumin (BSA), rhodamine 6G, new fuchsin, basic fuchsin, 3-mercaptopropanol, and Grace Bio-Labs CultureWell removable chambered coverglasses were purchased from Sigma-Aldrich (St. Louis, MO, USA). An EnzMet HRP detection kit for the immunohistochemistry assay was purchased from Nanoprobes (NY,

https://doi.org/10.1021/acsami.1c18815
ACS Appl. Mater. Interfaces 2021, 13, 58393−58400

USA). The antibodies including the anti-β-amyloid antibody, anti-tau antibody, and goat anti-rabbit IgG labeled with HRP were purchased from Abcam (Cambridge, England). The anti-GFAP antibody was purchased from Dako (Carpinteria, CA, USA). The anti-β-actin antibody was purchased from Cell Signaling Technology (Danvers, MA, USA). All reagents were used as received.

Formation of the Desert Rose-like Ag Nanostructures. Gold wafers were prepared by the vacuum deposition of a 15 nm-thick Cr film onto a silicon wafer followed by the deposition of a 100 nm-thick gold layer. As in a previous report, the gold wafers were cleaned by treatment with a super-piranha solution (20 mL of H_2O_2, 2 mL of HNO_3, and 12 mL of H_2SO_4).[41] To prepare a multi-well gold chip, 16-well CultureWell coverglasses were introduced onto the gold wafers. To immobilize HRP, 100 μL of HRP solution was added into each well (0.01 mg/mL in PBS). After washing with PBS five times, each gold chip-bottomed well was treated with Ag^+ ions in the presence of 0.2 mM Raman reporter for 2 min followed by the treatment of hydroquinone for 2 min and H_2O_2 for 10 min using an EnzMet HRP detection kit according to the manufacturer's instructions.

Mice. Tg-APPswe/PS1dE9 transgenic mice (APP/PS1 mice) were obtained from the Jackson Laboratory (Bar Harbor, ME, USA). The mice were maintained through cross-mating with C57BL/6J × C3H F1 hybrids. Mice not expressing the transgene were used as wild type controls. The animal room was maintained under specific-pathogen-free conditions, and the mice were housed in an environment with controlled temperature (21−22 °C) and humidity (50−60%) with a 12 h light/dark cycle (lights on at 7:00 AM). The mice were maintained on an ad libitum diet of lab chow (Teklad 2018S, Harlan, WI, USA) and had free access to water. Tg-APP/PS1 mice and wild type control mice at 9 months of age were used. All mice experiments were approved by the Institutional Animal Use and Care Committee of the Korea Research Institute of Bioscience and Biotechnology (KRIBB).

■ ASSOCIATED CONTENT

Supporting Information

The Supporting Information is available free of charge at https://pubs.acs.org/doi/10.1021/acsami.1c18815.

> Experimental details including miR-let7a detection, preparation of tissue samples, FDTA simulation, and Raman measurement; TEM and SEM images of nanostructures; and Raman measurement data for miR-let7a detection (PDF)

■ AUTHOR INFORMATION

Corresponding Authors

Tae Geol Lee − *Center for Nano-Bio Measurement, Korea Research Institute of Standards and Science (KRISS), Daejeon 34113, Korea; Department of Nano Science, University of Science and Technology (UST), Daejeon 34113, Korea;* orcid.org/0000-0002-6674-4147; Email: tglee@kriss.re.kr

Jung-Sub Wi − *Department of Materials Science and Engineering, Hanbat National University, Daejeon 34158, Korea;* orcid.org/0000-0002-9531-2001; Email: jungsub.wi@hanbat.ac.kr

Authors

Hee-Kyung Na − *Center for Nano-Bio Measurement, Korea Research Institute of Standards and Science (KRISS), Daejeon 34113, Korea*

Jisun Ki − *Center for Nano-Bio Measurement, Korea Research Institute of Standards and Science (KRISS), Daejeon 34113, Korea*

Minh-Uyen Le − *Center for Nano-Bio Measurement, Korea Research Institute of Standards and Science (KRISS), Daejeon 34113, Korea; Department of Nano Science, University of Science and Technology (UST), Daejeon 34113, Korea*

Kyoung-Shim Kim − *Laboratory Animal Resource Center, Korea Research Institute of Bioscience and Biotechnology (KRIBB), Daejeon 34141, Korea*

Chul-Ho Lee − *Laboratory Animal Resource Center, Korea Research Institute of Bioscience and Biotechnology (KRIBB), Daejeon 34141, Korea*

Complete contact information is available at: https://pubs.acs.org/10.1021/acsami.1c18815

Author Contributions

$^{\perp}$H.-K.N. and J.K. contributed equally to this paper. The manuscript was written through contributions of all authors. All authors have given approval to the final version of the manuscript.

Notes

The authors declare no competing financial interest.

■ ACKNOWLEDGMENTS

This work was supported by Development of Measurement Standards and Technology for Biomaterials and Medical Convergence funded by the Korea Research Institute of Standards and Science (KRISS-2021-GP2021-0004) and the Nano Material Technology Development Program (NRF-2014M3A7B6020163, NRF-2017M3A7B4041754, NRF-2018M3D1A1058814, and NRF-2021R1I1A3048262) of the National Research Foundation (NRF) of Korea.

■ REFERENCES

(1) Nie, S.; Emory, S. R. Probing Single Molecules and Single Nanoparticles by Surface-Enhanced Raman Scattering. *Science* **1997**, *275*, 1102−1106.

(2) Grubisha, D. S.; Lipert, R. J.; Park, H.-Y.; Driskell, J.; Porter, M. D. Femtomolar Detection of Prostate-Specific Antigen: An Immunoassay Based on Surface-Enhanced Raman Scattering and Immunogold Labels. *Anal. Chem.* **2003**, *75*, 5936−5943.

(3) Lane, L. A.; Qian, X.; Nie, S. SERS Nanoparticles in Medicine: From Label-Free Detection to Spectroscopic Tagging. *Chem. Rev.* **2015**, *115*, 10489−10529.

(4) Stiles, P. L.; Dieringer, J. A.; Shah, N. C.; Van Duyne, P. V. Surface-Enhanced Raman Spectroscopy. *Annu. Rev. Anal. Chem.* **2008**, *1*, 601−626.

(5) Gu, W.; Zhao, Y.; Zhuang, S.; Zha, J.; Dong, J.; You, Q.; Gan, Z.; Xia, N.; Li, J.; Deng, H.; Wu, Z. Unravelling the Structure of a Medium-Sized Metalloid Gold Nanocluster and its Filming Property. *Angew. Chem., Int. Ed.* **2021**, *60*, 11184−11189.

(6) Zong, C.; Xu, M.; Xu, L.-J.; Wei, T.; Ma, X.; Zheng, X.-S.; Hu, R.; Ren, B. Surface-Enhanced Raman Spectroscopy for Bioanalysis: Reliability and Challenges. *Chem. Rev.* **2018**, *118*, 4946−4980.

(7) Feng, M.; Tachikawa, H. Surface-Enhanced Resonance Raman Spectroscopic Characterization of the Protein Native Structure. *J. Am. Chem. Soc.* **2008**, *130*, 7443−7448.

(8) Wi, J.-S.; Barnard, E. S.; Wilson, R. J.; Zhang, M.; Tang, M.; Brongersma, M. L.; Wang, S. X. Sombrero-Shaped Plasmonic Nanoparticles with Molecular-Level Sensitivity and Multifunctionality. *ACS Nano* **2011**, *5*, 6449−6457.

(9) Matteini, P.; Cottat, M.; Tavanti, F.; Panfilova, E.; Scuderi, M.; Nicotra, G.; Menziani, M. C.; Khlebtsov, N.; De Angelis, M.; Pini, R. Site-Selective Surface-Enhanced Raman Detection of Proteins. *ACS Nano* **2017**, *11*, 918−926.

(10) Lee, S.; Lee, S.; Son, J.; Kim, J.-M.; Lee, J.; Yoo, S.; Haddadnezhad, M.; Shin, J.; Kim, J.; Nam, J.-M.; Park, S. Web-above-a-Ring (WAR) and Web-above-a-Lens (WAL): Nanostructures for Highly Engineered Plasmonic-Field Tuning and SERS Enhancement. *Small* **2021**, *17*, 2101262.
(11) Cao, Y. C.; Jin, R.; Nam, J.-M.; Thaxton, C. S.; Mirkin, C. A. Raman Dye-Labeled Nanoparticle Probes for Proteins. *J. Am. Chem. Soc.* **2003**, *125*, 14676−14677.
(12) Song, J.; Zhou, J.; Duan, H. Self-assembled plasmonic vesicles of SERS-Encoded Amphiphilic Gold Nanoparticles for Cancer Cell Targeting and Traceable Intracellular Drug Delivery. *J. Am. Chem. Soc.* **2012**, *134*, 13458−13469.
(13) Ma, S.; Li, Q.; Yin, Y.; Yang, J.; Liu, D. Interference-Free Surface-Enhanced Raman Scattering Tags for Single-Cell Molecular Imaging with a High Signal-to-Background Ratio. *Small* **2017**, *13*, 1603340.
(14) Lee, J.-H.; Oh, J.-W.; Nam, S. H.; Cha, Y. S.; Kim, G.-H.; Rhim, W.-K.; Kim, N. H.; Kim, J.; Han, S. W.; Suh, Y. D.; Nam, J.-M. Synthesis, Optical Properties, and Multiplexed Raman Bio-Imaging of Surface Roughness-Controlled Nanobridged Nanogap Particles. *Small* **2016**, *12*, 4726−4734.
(15) Taylor, R. W.; Lee, T.-C.; Scherman, O. A.; Esteban, R.; Aizpurua, J.; Huang, F. M.; Baumberg, J. J.; Mahajan, S. Precise Subnanometer Plasmonic Junctions for SERS within Gold Nanoparticle Assemblies using Cucurbit[n]uril "Glue". *ACS Nano* **2011**, *5*, 3878−3887.
(16) Shan, B.; Pu, Y.; Chen, Y.; Liao, M.; Li, M. Novel SERS labels: Rational design, functional integration and biomedical applications. *Coord. Chem. Rev.* **2018**, *371*, 11−37.
(17) Son, J. G.; Han, S. W.; Wi, J.-S.; Lee, T. G. Guided Formation of Sub-5 nm Interstitial Gaps between Plasmonic Nanodisks. *Nanoscale* **2015**, *7*, 8338−8342.
(18) Chao, J.; Cao, W.; Su, S.; Weng, L.; Song, S.; Fan, C.; Wang, L. Nanostructure-based Surface-Enhanced Raman Scattering Biosensors for Nucleic Acids and Proteins. *J. Mater. Chem. B* **2016**, 1757−1769.
(19) Xu, K.; Zhou, R.; Takei, K.; Hong, M. Toward Flexible Surface-Enhanced Raman Scattering (SERS) Sensors for Point-of-Care Diagnostics. *Adv. Sci.* **2019**, *6*, 1900925.
(20) Langer, J.; Jimenez de Aberasturi, D.; Aizpurua, J.; Alvarez-Puebla, R. A.; Auguié, B.; Baumberg, J. J.; Bazan, G. C.; Bell, S. E. J.; Boisen, A.; Brolo, A. G.; Choo, J.; Cialla-May, D.; Deckert, V.; Fabris, L.; Faulds, K.; García de Abajo, F. J.; Goodacre, R.; Graham, D.; Haes, A. J.; Haynes, C. L.; Huck, C.; Itoh, T.; Käll, M.; Kneipp, J.; Kotov, N. A.; Kuang, H.; Le Ru, E. C.; Lee, H. K.; Li, J.-F.; Ling, X. Y.; Maier, S. A.; Mayerhöfer, T.; Moskovits, M.; Murakoshi, K.; Nam, J.-M.; Nie, S.; Ozaki, Y.; Pastoriza-Santos, I.; Perez-Juste, J.; Popp, J.; Pucci, A.; Reich, S.; Ren, B.; Schatz, G. C.; Shegai, T.; Schlücker, S.; Tay, L.-L.; Thomas, K. G.; Tian, Z.-Q.; Van Duyne, R. P.; Vo-Dinh, T.; Wang, Y.; Willets, K. A.; Xu, C.; Xu, H.; Xu, Y.; Yamamoto, Y. S.; Zhao, B.; Liz-Marzán, L. M. Present and Future of Surface-Enhanced Raman Scattering. *ACS Nano* **2020**, *14*, 28−117.
(21) Wang, Z.; Zong, S.; Wu, L.; Zhu, D.; Cui, Y. SERS-Activated Platforms for Immunoassay: Probes, Encoding Methods, and Applications. *Chem. Rev.* **2017**, *117*, 7910−7963.
(22) Yüksel, S.; Ziegler, M.; Goerke, S.; Hübner, U.; Pollok, K.; Langenhorst, F.; Weber, K.; Cialla-May, D.; Popp, J. Background-Free Bottom-Up Plasmonic Arrays with Increased Sensitivity, Specificity and Shelf Life for SERS Detection Schemes. *J. Phys. Chem. C* **2015**, *119*, 13791−13798.
(23) Arabi, M.; Ostovan, A.; Zhang, Z.; Wang, Y.; Mei, R.; Fu, L.; Wang, X.; Ma, J.; Chen, L. Label-free SERS detection of Raman-Inactive protein biomarkers by Raman reporter indicator: Toward ultrasensitivity and universality. *Biosens. Bioelectron.* **2021**, *174*, 112825.
(24) Nanda Kumar, D.; Chandrasekaran, N.; Mukherjee, A. Horseradish Peroxidase-Mediated In Situ Synthesis of Silver Nanoparticles: Application for Sensing of Mercury. *New J. Chem.* **2018**, *42*, 13763−13769.
(25) Van Den Pol, A. N. Tyrosine Hydroxylase Immunoreactive Neurons Throughout the Hypothalamus Receive Glutamate Decarboxylase Immunoreactive Synapses: A Double Pre-embedding Immunocytochemical Study with Particulate Silver and HRP. *J. Neurosci.* **1986**, *6*, 877−891.
(26) Liu, R.; Sen, A. Unified Synthetic Approach to Silver Nanostructures by Galvanic Displacement Reaction on Copper: From Nanobelts to Nanoshells. *Chem. Mater.* **2012**, *24*, 48−54.
(27) Chhatre, A.; Thaokar, R.; Mehra, A. Formation of Gold Nanorods by Seeded Growth: Mechanisms and Modeling. *Cryst. Growth Des.* **2018**, *18*, 3269−3282.
(28) Chang, Y.-H.; Liu, C.; Rouvimov, S.; Luo, T.; Feng, S.-P. Electrochemical Synthesis to Convert a Ag film into Ag Nanoflowers with High Electrocatalytic Activity. *Chem. Commun.* **2017**, *53*, 6752−6755.
(29) Duchene, J. S.; Niu, W.; Abendroth, J. M.; Sun, Q.; Zhao, W.; Huo, F.; Wei, W. D. Halide Anions as Shape-Directing Agents for Obtaining High-Quality Anisotropic Gold Nanostructures. *Chem. Mater.* **2013**, *25*, 1392−1399.
(30) Poolakkandy, R. R.; Menamparambath, M. M. Soft-Template-Assisted Synthesis: a Promising Approach for the Fabrication of Transition Metal Oxides. *Nanoscale Adv.* **2020**, *2*, 5015−5045.
(31) Karunakaran, S. C.; Cafferty, B. J.; Jain, K. S.; Schuster, G. B.; Hud, N. V. Reversible Transformation of a Supramolecular Hydrogel by Redox Switching of Methylene Blue-A Noncovalent Chain Stopper. *ACS Omega* **2019**, *5*, 344−349.
(32) Kneipp, K.; Moskovits, M.; Kneipp, H. *Surface-Enhanced Raman Scattering: Physics and Applications*. Ed.; Springer: Berlin, Heidelberg, New York. 2006.
(33) Wu, J.; Tan, L. H.; Hwang, K.; Xing, H.; Wu, P.; Li, W.; Lu, Y. DNA Sequence-Dependent Morphological Evolution of Silver Nanoparticles and Their Optical and Hybridization Properties. *J. Am. Chem. Soc.* **2014**, *136*, 15195−15202.
(34) Hamad, M. T. Biosynthesis of Silver Nanoparticles by Fungi and Their Antibacterial Activity. *Int. J. Environ. Sci. Technol.* **2019**, *16*, 1015−1024.
(35) Chen, H.; Park, S.-G.; Choi, N.; Moon, J.-I.; Dang, H.; Das, A.; Lee, S.; Kim, D.-G.; Chen, L.; Choo, J. SERS Imaging-based Aptasensor for Ultrasensitive and Reproducible Detection of Influenza Virus A. *Biosens. Bioelectron.* **2020**, *167*, 112496.
(36) Zhao, M.; Guo, H.; Liu, W.; Tang, J.; Wang, L.; Zhang, B.; Xue, C.; Liu, J.; Zhang, W. Silica Cladding of Ag Nanoparticles for High Stability and Surface-Enhanced Raman Spectroscopy Performance. *Nanoscale Res. Lett.* **2016**, *11*, 403.
(37) Cummings, B. J.; Pike, C. J.; Shankle, R.; Cotman, C. W. β-amyloid Deposition and Other Measures of Neuropathology Predict Cognitive Status in Alzheimer's Disease. *Neurobiol. Aging* **1996**, *17*, 921−933.
(38) Kraft, A. W.; Hu, X.; Yoon, H.; Yan, P.; Xiao, Q.; Wang, Y.; Gil, S. C.; Brown, J.; Wilhelmsson, U.; Restivo, J. L.; Cirrito, J. R.; Holtzman, D. M.; Kim, J.; Pekny, M.; Lee, J.-M. Attenuating Astrocyte Activation Accelerates Plaque Pathogenesis in APP/PS1 Mice. *FASEB J.* **2013**, *27*, 187−198.
(39) Wiercigroch, E.; Stepula, E.; Mateuszuk, L.; Zhang, Y.; Baranska, M.; Chlopicki, S.; Schlücker, S.; Malek, K. ImmunoSERS Microscopy for the Detection of Smooth Muscle Cells in Atherosclerotic Plaques. *Biosens. Bioelectron.* **2019**, *133*, 79−85.
(40) Zhang, Y.; Gu, Y.; He, J. B. D.; Thackray, Y. J.; Ye, J. Ultrabright Gap-Enhanced Raman Tags for High-Speed Bioimaging. *Nat. Commun.* **2019**, *10*, 3905.
(41) Na, H.-K.; Shon, H. K.; Son, H. Y.; Jang, E.; Joh, S.; Huh, Y.-M.; Castner, D. G.; Lee, T. G. Utilization of Chromogenic Enzyme Substrates for Signal Amplification in Multiplexed Detection of Biomolecules using Surface Mass Spectrometry. *Sens. Actuators B Chem.* **2021**, *332*, 129452.

https://doi.org/10.1021/acsami.1c18815
ACS Appl. Mater. Interfaces 2021, 13, 58393−58400